Chinese Chemical Letters 35 (2024) 108474

Contents lists available at ScienceDirect

Chinese Chemical Letters

journal homepage: www.elsevier.com/locate/cclet

Construction of biomimetic proton transport channels in metal-organic framework

Xiao-Min Li[a,*], Junchao Jia[a], Danting Yang[b], Jiali Jin[b], Junkuo Gao[a,*]

[a] School of Materials Science and Engineering, Institute of Functional Porous Materials, Zhejiang Sci-Tech University, Hangzhou 310018, China
[b] Zhejiang Key Laboratory of Pathophysiology, School of Public Health, School of Medicine, Ningbo University, Ningbo 315211, China

ARTICLE INFO

Article history:
Received 30 January 2023
Revised 16 February 2023
Accepted 18 April 2023
Available online 19 April 2023

Keywords:
MOF
Amino acids
Biomimetic proton transport channels
Synergistic effect
Proton conduction mechanism

ABSTRACT

Construction of proton transport channels in metal-organic frameworks (MOFs) with simple synthesis processes, high proton conductivities and good performance stabilities has been of great interest for proton exchange membrane fuel cell (PEMFC). Herein, we mimic the proton transport behavior of amino acid residues in bacteriorhodopsin, select UiO-66-COOH as the host, glycine and aspartic acid as the functional guest molecules, and then functionalize the MOF framework with amino acids to obtain biomimetic proton transport channels. This strategy endows UiO-66-COOH-Asp a high proton conductivity of 1.19×10^{-2} S/cm at 70 °C and 98% RH, excellent cycle stability of performances and performance durability, which can be comparable to the reported MOFs-based proton conductors. Moreover, the proton conduction mechanism in UiO-66-COOH-Asp is elaborated in detail due to its visual structure, which is also one of the advantages of adopting MOFs as research platform, making it possible to optimize the structure-activity relationship of advanced materials. Notably, this strategy has clear objectives and simple synthesis, which has made certain contributions to both theoretical research and future industrial production of proton conductors.

Energy depletion and global warming are the two most serious challenges facing society today [1,2]. To meet these challenges, researchers around the world are exploring alternative energy sources [3], among which proton exchange membrane fuel cell (PEMFC) is a promising clean energy device due to its ultralow emission and high power density [4–7]. Constructing highly effective and stable proton transport channel is very indispensable for developing proton exchange membrane (PEM), that is a core component of PEMFC [8,9]. Currently, the most commonly used PEM is Nafion, but it has the defects of difficult preparation, high cost and amorphous [10–14]. Thus, it has always been the goal of researchers to seek alternatives to Nafion. Metal-organic framework (MOF) has made great contributions to the visual exploration of hydrogen bond network and the improvement of proton conductivity due to its unique structure and functional organic linker [15,16]. Moreover, the simple and cheap synthesis process of MOF makes its large-scale production possible [17]. Therefore, MOF is a good platform for studying proton conduction behavior, among which it is worth noting that the construction of intrinsic proton transport network obtained by modifying MOFs frameworks with functional molecules is more meaningful for exploring stable MOFs based proton conductors [18,19].

Proton transfer is a ubiquitous and significant process in organisms. Inspired by biological proton channels, biomimetic proton transport channels have attracted great research interest [20] and have been widely used in the fields of biosensors [21–23] and ion separation [24–26]. However, the works on the efficient proton transport pathways in PEMs constructed by biomimetic proton channels still need to be expanded, which can accumulate research examples and provide more theoretical basis for further practical applications. Specifically, amino acids are important organic molecules in biology, which can achieve efficient proton transfer, resulting in making them become good candidates as functional molecules to participate in the construction of biomimetic proton transport paths [27,28].

Considering the above, combining MOFs with amino acids may become a general and effective strategy. Based on this, we mimic the proton transport behavior of amino acid residues in bacteriorhodopsin, [29] select UiO-66-COOH as the host, glycine and aspartic acid as the functional guest molecules, and then functionalize the MOF framework with amino acids to obtain biomimetic proton transport channels (Scheme 1). UiO-66-COOH reacts with

* Corresponding authors.
E-mail addresses: lixm@zstu.edu.cn (X.-M. Li), jkgao@zstu.edu.cn (J. Gao).

https://doi.org/10.1016/j.cclet.2023.108474
1001-8417/

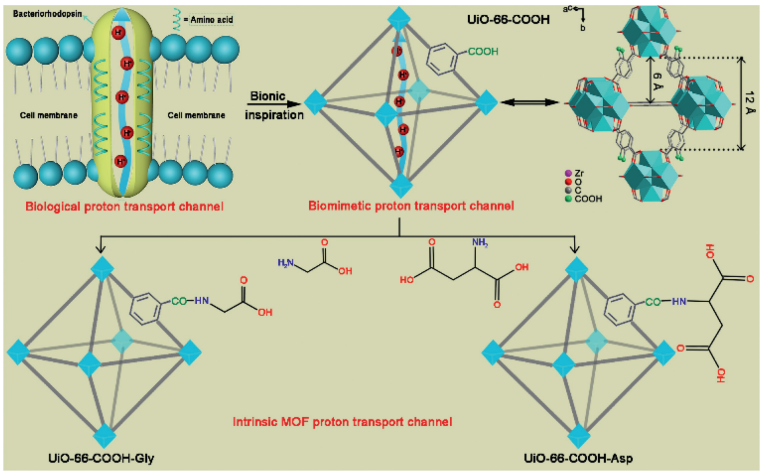

Scheme 1. Schematic illustration of the preparations of UiO-66-COOH-Gly and UiO-66-COOH-Asp.

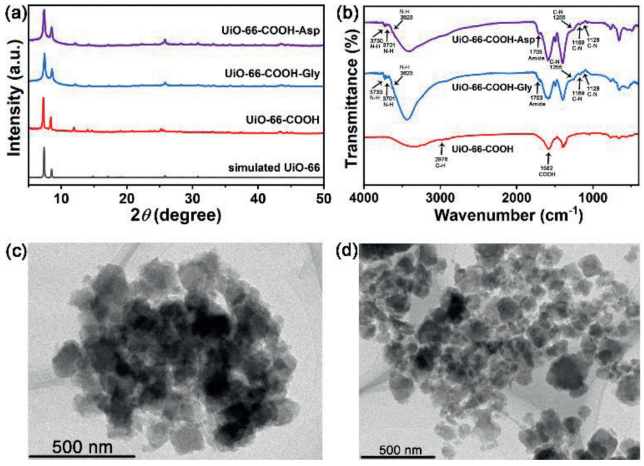

Fig. 1. (a) PXRD patterns of simulated UiO-66-COOH (gray), as-synthesized UiO-66-COOH (red), as-synthesized UiO-66-COOH-Gly (blue) and as-synthesized UiO-66-COOH-Asp (violet). (b) FT-IR spectra of as-synthesized UiO-66-COOH (red), as-synthesized UiO-66-COOH-Gly (blue) and as-synthesized UiO-66-COOH-Asp (violet). (c) TEM image of as-synthesized UiO-66-COOH-Gly. (d) TEM image of as-synthesized UiO-66-COOH-Asp.

glycine and aspartic acid to form UiO-66-COOH-Gly and UiO-66-COOH-Asp, respectively, through amide reaction. Because of imide group (served as proton receiver) and carboxylic acid group (served as proton donor) in UiO-66-COOH-Gly and UiO-66-COOH-Asp, they exhibit proton conductivities of 4.9×10^{-3} S/cm and 1.19×10^{-2} S/cm at 70 °C and 98% RH, respectively, with assist of water molecules from humidifier. It is worth noting that the proton conductivity of UiO-66-COOH-Asp is one order of magnitude higher than that of UiO-66-COOH-Gly, which shows that carboxylic acid group is advantageous to proton transport.

According to the published literature, we synthesized UiO-66-COOH as the initial material, and then synthesized UiO-66-COOH-Gly and UiO-66-COOH-Asp with glycine and aspartic acid, respectively, through amide reaction. As shown in Fig. 1a, the PXRD patterns of UiO-66-COOH, UiO-66-COOH-Gly and UiO-66-COOH-Asp fit well with that of simulated UiO-66, which not only proves that the three materials have high purities, but also proves that the post-modified materials retain the structural framework of UiO-66-COOH. These typical peaks of O–H vibration and COOH vibration extracted from Fourier-transform infrared (FTIR) spectroscopy of UiO-66-COOH also show that UiO-66-COOH has been successfully prepared (Fig. 1b and Fig. S1 in Supporting information) [30]. The morphologies of UiO-66-COOH, UiO-66-COOH-Gly and UiO-66-COOH-Asp were detected by scanning electron microscope (SEM) and transmission electron microscopy (TEM) measurements shown in Figs. S2-S5 (Supporting information) and Figs. 1c and d, from which it can be seen that UiO-66-COOH-Gly and UiO-66-COOH-Asp almost keep the morphological feature of UiO-66-COOH.

In order to testify the successful modification of UiO-66-COOH-Gly and UiO-66-COOH-Asp, we employed a variety of characterization methods. As shown in Figs. S6-S11 (Supporting information), their elemental distribution mapping images and energy dispersive X-ray (EDX) spectra demonstrate that UiO-66-COOH-Gly and UiO-66-COOH-Asp have nitrogen element originating from amino acids compared with UiO-66-COOH, which is an indirect proof that amino acids modified the MOF framework. Furthermore, FTIR spectra of UiO-66-COOH-Gly and UiO-66-COOH-Asp were conducted, and the results are displayed in Fig. 1b. It can be observed that there are new bands at 3730, 3701 and 3623 cm^{-1} in UiO-66-COOH-Gly and UiO-66-COOH-Asp compared with that in UiO-66-COOH, which are the sign of N–H stretching vibration [31–33], suggesting that the amino groups of amino acids react with the carboxylic acid groups of UiO-66-COOH. Similarly, the emerging bands located at 1255, 1169 and 1128 cm^{-1} in UiO-66-COOH-Gly and UiO-66-COOH-Asp are ascribed to C–N stretching vibration [31,32], which indicates the successful amide reaction between UiO-66-COOH and amino acids. The amide vibrational peaks at 1703 cm^{-1} in UiO-66-COOH-Gly and UiO-66-COOH-Asp, respectively, further prove that amino acids were involved in the amide reaction with carboxylic acid groups of UiO-66-COOH [34–36]. Additionally, Raman measurements were performed to confirm the successful syntheses of UiO-66-COOH-Gly and UiO-66-COOH-Asp. It can be seen from Fig. S12 (Supporting information) that the Raman spectra of UiO-66-COOH-Gly and UiO-66-COOH-Asp emerge three new peaks located at 1256, 1301 and 1493 cm^{-1}, respectively, assigning to amide (C–N stretching mode and N–H stretching mode) [37,38], which is powerful evidence for the successful post modification. Moreover, the X-ray photoelectron spectroscopy (XPS) measurements of UiO-66-COOH, UiO-66-COOH-Gly and UiO-66-COOH-Asp were conducted (Fig. S13 in Supporting information). It can be seen from Fig. S14 (Supporting information) that there are new peaks at the bonding energy of 288.8 eV in C 1s spectra of UiO-66-COOH-Gly and UiO-66-COOH-Asp compared with those of UiO-66-COOH, which can be assigned to O=C–N, showing that amino acids have been successfully combined with UiO-66-COOH

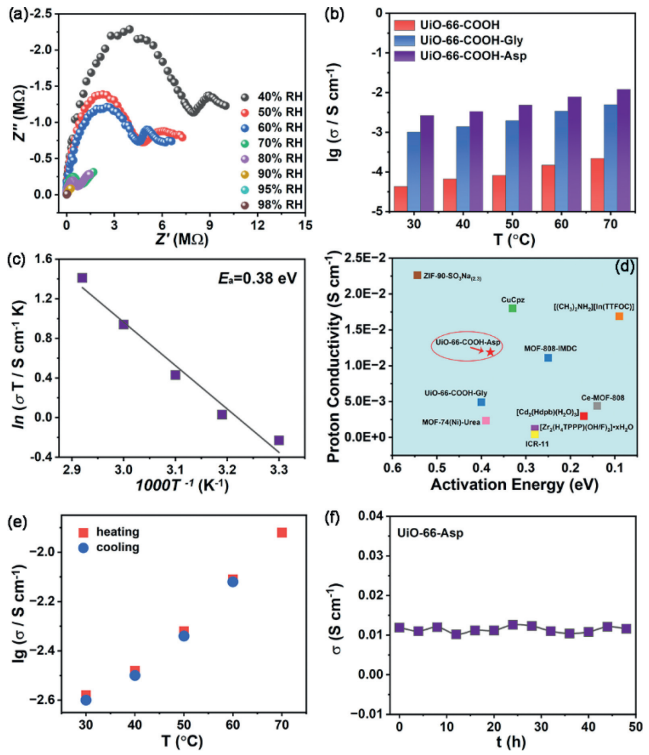

Fig. 2. (a) Nyquist plots from AC impedance data of UiO-66-COOH-Asp at 30 °C and different humidities variation from 40% to 98% RH. (b) Temperature-dependent proton conductivities of UiO-66-COOH (red), UiO-66-COOH-Gly (blue) and UiO-66-COOH-Asp (violet) (98% RH, 30–70 °C). (c) Arrhenius plot of UiO-66-COOH-Asp under 98% RH and in the temperature range of 30–70 °C. (d) Comparison of the proton conductivities and activation energies of UiO-66-COOH-Gly, UiO-66-COOH-Asp and some other MOFs-based proton conductors published in recent two years. (e) The proton conductivities for the heating-cooling cycle of UiO-66-COOH-Asp at 98% RH and within the temperature range of 30–70 °C. (f) The time-dependent proton conductivities of UiO-66-COOH-Asp measured at 70 °C and 98% RH.

framework [39,40]. Similarly, there are new peaks at the bonding energy of 399.9 eV in N 1s spectra of UiO-66-COOH-Gly and UiO-66-COOH-Asp, which can be assigned to -NH-, indicating that amide reaction occurred (Fig. S15 in Supporting information) [41]. As a further proof, N_2 adsorption-desorption tests of UiO-66-COOH, UiO-66-COOH-Gly and UiO-66-COOH-Asp were measured. The N_2 adsorption capacities of UiO-66-COOH-Gly and UiO-66-COOH-Asp are lower than that of UiO-66-COOH, which shows that the functional molecules (amino acids) have occupied the pores of UiO-66-COOH (Fig. S16 in Supporting information). It can be sufficiently concluded that amino acids have modified UiO-66-COOH skeleton through amide reaction to obtain UiO-66-COOH-Gly and UiO-66-COOH-Asp. Last but not least, the thermogravimetric (TG) curves of the three materials were also detected. As shown in Figs. S17-S19 (Supporting information), the first weight loss originating from solvent molecules occurred at nearly 200 °C, and the three materials can keep their structures stable until above 350 °C. It can be known that they have enough thermal stabilities, which provides a guarantee for subsequent proton conductivity measurements.

To evaluate the proton conduction performances of designed materials, we first measured alternating current (AC) impedance spectra at 30 °C and different humidities from 40% RH to 98% RH (Figs. S20-S22 in Supporting information and Fig. 2a). With the humidity increases, the proton conductivity increases as well until the humidity reaches the maximum value of 98% RH, which indicates that water molecules provided by the humidifier participate in proton transport (Figs. S23-S25 in Supporting information). At low humidity, there is almost no water molecule to participate in proton transport. When humidity increases, water molecules can cooperate with proton carriers originating from MOF framework to promote highly efficient proton transport. At 30 °C and 98% RH, the proton conductivities of UiO-66-COOH, UiO-66-COOH-Gly and UiO-66-COOH-Asp are 4.24×10^{-5}, 9.94×10^{-4} and 2.62×10^{-3} S/cm, respectively, among which it can be clearly seen that amino acids play a positive role in proton transport in MOF. Notably, the proton conductivity of UiO-66-COOH-Asp is one order of magnitude higher than that of UiO-66-COOH-Gly-due to more abundant carboxylic acid groups stemming from UiO-66-COOH-Asp.

To explore the effect of temperature on proton conductivity, the temperature-dependent curves of the three materials were also measured at 98% RH and within the temperature range of 30–70 °C (Figs. S26, S27 and S28a in Supporting information). The Nyquist plots of UiO-66-COOH in Fig. S26 display two semicircles located at high frequency region and a tail located at low frequency region, in which the former is attributed to the bulk resistance and grain boundary resistance and the latter is attributed to the mobile ions blocked at the interfaces between electrode and electrolyte [42]. Consequently, the front semicircle was chosen to calculate the proton conductivity. Similarly, the temperature has a positive influence on proton transfer and the proton conductivity reaches the maximum value at 70 °C. Specifically, the proton conductivities of UiO-66-COOH, UiO-66-COOH-Gly and UiO-66-COOH-Asp at 70 °C and 98% RH are 2.17×10^{-4}, 4.90×10^{-3} and 1.19×10^{-2} S/cm, respectively. As shown in Fig. 2b, UiO-66-COOH-Asp has the most advantage in proton conductivity, which is because that its biomimetic proton transport channel has highly efficient hydrogen bond networks synergistically constructed by carboxylic acid groups, amide groups and water molecules.

To understand the proton transport mechanism in the three materials, the activation energies (E_a) of UiO-66-COOH, UiO-66-COOH-Gly and UiO-66-COOH-Asp were calculated from Arrhenius equation, and the results show that their E_a values are 0.41, 0.40 and 0.38 eV, respectively (Figs. S29 and S30 in Supporting information, Fig. 2c). The activation energy of UiO-66-COOH is larger than 0.40 eV, belonging to the vehicle mechanism. While the activation energies of UiO-66-COOH-Gly and UiO-66-COOH-Asp are in the range of 0–0.40 eV, belonging to the Grotthuss mechanism. Moreover, the E_a value of UiO-66-COOH-Asp is the smallest, indicating that more rapid proton transport is carried out in the proton channels of UiO-66-COOH-Asp, which is also the reason for the highest proton conductivity obtained by UiO-66-COOH-Asp. Combining proton conductivity and activation energy, it can be seen the advantageous status of UiO-66-COOH-Asp in the recently published MOFs-based proton conductors (Fig. 2d), and the specific values and references are listed in Table S1 (Supporting information). Importantly, this is also an example of people learning from nature and living organisms.

The excellent cycle stability and durability of performance are the prerequisites for further application. Therefore, we further tested the temperature cycle stability (Fig. S28 in Supporting information) and durability of UiO-66-COOH-Asp. Fig. 2e shows that at 98% RH, the proton conductivity at each temperature in the heating stage is almost the same as that at the corresponding temperature in the cooling stage, which demonstrates that UiO-66-COOH-Asp has excellent cycle stability. Moreover, there is negligible difference in activation energy of UiO-66-COOH-Asp between the heating stage and the cooling stage (Fig. S31 in Supporting information). Simultaneously, it can be seen from the durability test results that the proton conductivity of UiO-66-COOH-Asp hardly degrades after 48 h at 70 °C and 98% RH (Fig. 2f). Besides, it can be seen from the PXRD patterns after undergoing tests that the materials have excellent structural stabilities (Fig. S32 in Supporting information). These results suggest that UiO-66-COOH-Asp has

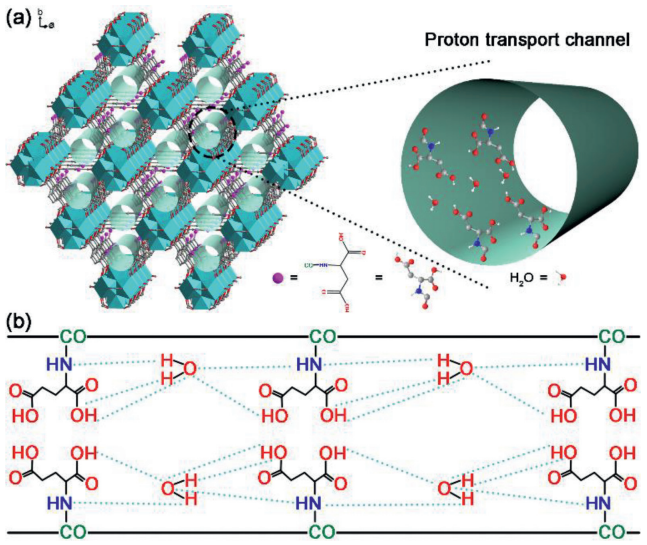

Fig. 3. (a) Possible proton transport channel with multiple proton carriers of UiO-66-COOH-Asp. (b) Schematic representation of the possible proton hopping routes in UiO-66-COOH-Asp.

a strong potential in the follow-up application exploration, which again shows the great significance of bionics.

Understanding the mechanism will contribute to the development of expected materials including their preset structure and the improvement of their structure-activity relationship. This is also an important reason why MOF is one of the candidates for studying proton conduction. As shown in Fig. 3a, UiO-66-COOH-Asp has many regular pores that can be used as proton transport channels. In addition, abundant proton carriers are arranged in the cavities of UiO-66-COOH-Asp to construct fast biomimetic proton transport channels due to the introduction of aspartic acid. The possible proton hopping routes are presented in Fig. 3b. With the assistance of water molecules in the environment, it is intuitive to observe that the proton hopping pathways in UiO-66-COOH-Asp are diverse, which can promote proton transport. Specifically, carboxylic acid groups, amide and water molecules can provide protons as proton donors, and they can receive protons as proton receptors simultaneously. The hydrophilic carboxylic acid group is very conductive to the rapid proton transport, because it is easy to provide dissociated proton in high humidity, which is why the proton conductivity of UiO-66-COOH-Asp is higher than that of UiO-66-COOH-Gly. Moreover, compared with UiO-66-COOH-Gly, UiO-66-COOH-Asp has more carboxylic acid groups that provide both proton sources and proton hopping sites, which can cooperate with water molecules and amide groups to synergistically build super-efficient proton transport networks. Overall, the strategy of using MOF to construct biomimetic proton transport channels proposed by us can make the target product obtain high proton conductivity, and the visual structure of MOF can make researchers better understand the proton transfer mechanism, which contributes to the directional construction of proton transport.

In summary, biomimetic proton transport channels have been constructed by modifying UiO-66-COOH with amino acids to realize high proton conductivities. The obtained UiO-66-COOH-Asp shows 1.19×10^{-2} S/cm at 70 °C and 98% RH, which is 55 times of UiO-66-COOH and 2.4 times of UiO-66-COOH-Gly. It is also found that the proton transport in UiO-66-COOH-Asp belongs to the Grotthuss mechanism, which indicates that fast proton transfer occurs in the biomimetic proton transport channels. Moreover, UiO-66-COOH-Asp has good cycle stability and durability of performance. These results prove that UiO-66-COOH-Asp is an excellent proton conductor, which provides a basis for further practical application. Importantly, the structure visualization of MOFs also provides a good platform for studying the structure-activity relationship of proton conduction, which promotes the development of a kind of advanced material. It is worth mentioning that this strategy has clear objectives and simple synthesis, which has made certain contributions to both theoretical research and future industrial production of proton conductors. At the same time, it is also an example of human learning from nature living organisms.

Declaration of competing interest

The authors declare that they have no known competing financial interests or personal relationships that could have appeared to influence the work reported in this paper.

Acknowledgments

This work was supported by the Zhejiang Provincial Natural Science Foundation of China (No. LY20E020001), Research Initiation Fund Project from Zhejiang Sci-Tech University (No. 22212154-Y) and the Fundamental Research Funds of Zhejiang Sci-Tech University (No. 22212290-Y).

Supplementary materials

Supplementary material associated with this article can be found, in the online version, at doi:10.1016/j.cclet.2023.108474.

References

[1] S.C. Pal, M.C. Das, Adv. Funct. Mater. 31 (2021) 2101584.
[2] Y. Wu, Y. Li, J. Gao, Q. Zhang, SusMat 1 (2021) 66–87.
[3] Y. Li, Y. Wu, T. Li, et al., Carbon Energy 5 (2023) e265.
[4] X.M. Li, J. Liu, C. Zhao, et al., J. Mater. Chem. A 7 (2019) 25165–25171.
[5] Y. Ye, W. Guo, L. Wang, et al., J. Am. Chem. Soc. 139 (2017) 15604–15607.
[6] H. Jin, S. Zou, Q. Wen, et al., Chin. Chem. Lett. 34 (2023) 107441.
[7] K. Wang, N. Li, Y. Yang, et al., Chin. Chem. Lett. 32 (2021) 3159–3163.
[8] X.M. Li, L.Z. Dong, J. Liu, et al., Chem 6 (2020) 2272–2282.
[9] Y.R. Liu, Y.Y. Chen, Q. Zhuang, G. Li, Coord. Chem. Rev. 471 (2022) 214740.
[10] Y. Zhai, H. Zhang, J. Hu, B. Yi, J. Membr. Sci. 280 (2006) 148–155.
[11] G. He, J. Zhao, S. Hu, et al., ACS Appl. Mater. Interfaces 6 (2014) 15291–15301.
[12] K.S. Lee, J.S. Spendelow, Y.K. Choe, C. Fujimoto, Y.S. Kim, Nat. Energy 1 (2016) 16120.
[13] X.M. Li, L.Z. Dong, S.L. Li, et al., ACS Energy Lett. 2 (2017) 2313–2318.
[14] X.M. Li, J. Gao, SusMat 2 (2022) 504–534.
[15] D.W. Lim, M. Sadakiyo, H. Kitagawa, Chem. Sci. 10 (2019) 16–33.
[16] Z. Zhang, Q. Han, S. Zhang, et al., ACS Sustain. Chem. Eng. 10 (2022) 11867–11874.
[17] K. Pobłocki, J. Drzeżdżon, B. Gawdzik, D. Jacewicz, Green Chem. 24 (2022) 9402–9427.
[18] D.W. Kang, M. Kang, C.S. Hong, J. Mater. Chem. A 8 (2020) 7474–7494.
[19] X.M. Li, Y. Wang, Y. Mu, J. Gao, L. Zeng, J. Mater. Chem. A 10 (2022) 18592–18597.
[20] J. Hao, W. Wang, J. Zhao, et al., Chin. Chem. Lett. 33 (2022) 2291–2300.
[21] C.R. Martin, Z.S. Siwy, Science 317 (2007) 331–332.
[22] Z. Zhang, L. Wen, L. Jiang, Chem. Soc. Rev. 47 (2018) 322–356.
[23] L. Mayne, C.Y. Lin, S.D.R. Christie, Z.S. Siwy, M. Platt, ACS Nano 12 (2018) 4844–4852.
[24] L.A. Baker, S.P. Bird, Nat. Nanotechnol. 3 (2008) 73–74.
[25] X. Li, H. Zhang, P. Wang, et al., Nat. Commun. 10 (2019) 2490.
[26] P. Wang, M. Wang, F. Liu, et al., Nat. Commun. 9 (2018) 569.
[27] R. Nandi, Y. Agam, N. Amdursky, Adv. Mater. 33 (2021) 2101208.
[28] Y. Li, J. Dong, W. Gong, et al., J. Am. Chem. Soc. 143 (2021) 20939–20951.
[29] C. Kandt, K. Gerwert, J. Schlitter, Proteins 58 (2005) 528–537.
[30] F. Liu, W. Xiong, X. Feng, et al., Environ. Technol. 41 (2020) 3094–3104.
[31] A.C. Sadiq, N.Y. Rahim, F.B.M. Suah, Int. J. Biol. Macromol. 164 (2020) 3965–3973.
[32] H.B. Luo, Q. Ren, P. Wang, et al., ACS Appl. Mater. Interfaces 11 (2019) 9164–9171.
[33] A. Sharma, J. Lim, S. Jeong, et al., Angew. Chem. Int. Ed. 60 (2021) 14334–14338.
[34] A. Bouhekka, T. Bürgi, Appl. Surf. Sci. 261 (2012) 369–374.
[35] E. Beilis, B. Belgorodsky, L. Fadeev, H. Cohen, S. Richter, J. Am. Chem. Soc. 136 (2014) 6151–6154.
[36] J. Grdadolnik, Y. Maréchal, Biopolymers 62 (2001) 40–53.

[37] S.K. Srivastava, A.K. Ojha, W. Kiefer, B.P. Asthana, Spectrochim. Acta A 61 (2005) 2832–2839.
[38] C. Mensch, P. Bultinck, C. Johannessen, Phys. Chem. Chem. Phys. 21 (2019) 1988–2005.
[39] S.K. Das, C. Dickinson, F. Lafir, D.F. Brougham, E. Marsili, Green Chem. 14 (2012) 1322–1334.
[40] P.R. Sreenath, S. Mandal, H. Panigrahi, P. Das, K.D. Kumar, Nano Struct. Nano Objects 23 (2020) 100477.
[41] P.R. Sreenath, S. Singh, M.S. Satyanarayana, P. Das, K.D. Kumar, Polymer 112 (2017) 189–200 Guildf.
[42] V.G. Ponomareva, K.A. Kovalenko, A.P. Chupakhin, et al., J. Am. Chem. Soc. 134 (2012) 15640–15643.